HHS Public Access

Author manuscript

J Autoimmun. Author manuscript; available in PMC 2019 July 01.

Published in final edited form as:

J Autoimmun. 2018 July ; 91: 34–44. doi:10.1016/j.jaut.2018.03.001.

Mechanisms of Neuropsychiatric Lupus: The Relative Roles of the Blood-CSF versus Blood-Brain Barrier

Sivan Gelb[1], **Ariel D. Stock**[2], **Shira Anzi**[1], **Chaim Putterman**[2], and **Ayal Ben-Zvi**[1,*]

[1]Department of Developmental Biology and Cancer Research, The Institute for Medical Research Israel-Canada, Faculty of Medicine, Hebrew University of Jerusalem, Jerusalem 91120, Israel

[2]Division of Rheumatology and Department of Microbiology and Immunology, Albert Einstein College of Medicine, Bronx, NY 10461, USA

Abstract

The pathogenesis of neuropsychiatric lupus (NPSLE) is believed to include the entry of circulating neuropathic antibodies to the brain via a pathologically permeable blood-brain barrier (BBB). Nevertheless, direct evidence of BBB pathology or mechanisms underlying BBB dysfunction is missing. Here, we examined BBB integrity in an established NPSLE mouse model (MRL/*fas*$^{lpr/lpr}$). Surprisingly, challenging the barrier with various exogenous tracers demonstrated insignificant changes in BBB permeability. Furthermore, electron microscopy showed no ultrastructure changes supporting hyper-permeability. However, we found that abnormal function of the Blood-Cerebrospinal Fluid Barrier (BCSFB) in the choroid plexus underlies brain exposure to neuropathic antibodies. Considerable intrathecal lymphocyte infiltration likely occurs through the BCSFB, accompanied by epithelial hyper-permeability to antibodies. Our results challenge the commonly held view of BBB disruption in NPSLE, supporting a shift in focus to BCSFB dysfunction as a causative factor in the disease.

Keywords

Lupus; neuropsychiatric-lupus (NPSLE); blood-brain barrier (BBB); blood-CSF barrier (BCSFB); autoantibodies; choroid plexus (CP)

Address correspondence to: Ayal Ben-Zvi, PhD, Department of Developmental Biology and Cancer Research, The Institute for Medical Research Israel-Canada, Faculty of Medicine, Hebrew University of Jerusalem, Jerusalem 91120, Israel, Tel: +972-2-6787624, Ayalb@ekmd.huji.ac.il.

Contributors

S.G, C.P, and A.B.Z designed research, S.G, A.D.S, and S.A performed research, S.G analyzed data, S.G, C.P, and A.B.Z wrote the paper, with critical input from A.D.S.

Competing interests

None.

1. Introduction

Systemic lupus erythematosus (SLE) is an autoimmune disease that can cause multi-organ damage frequently involving skin, kidney, lung, heart and brain[1–3]. The disease is characterized by loss of tolerance to self-antigens, formation of autoantibodies, and immunological complex deposition followed by leukocyte activation and cytokine production causing systemic inflammation and tissue damage[4,5]. Patients with SLE that manifest from one or more of several neuropsychiatric symptoms are classified as 'neuropsychiatric lupus' (NPSLE)[6]. NPSLE is perhaps the least understood but one of the most prevalent manifestation in lupus, which may occur independently of active systemic disease and without serologic activity[4]. There is substantial evidence indicating that NPSLE can be a primary manifestation of brain inflammatory disease, rather than simply an outcome of end-organ dysfunction and/or treatment. Moreover, NPSLE can occur when the systemic disease is absent or stable[6]. The American College of Rheumatology (ACR) defined 19 neuropsychiatric syndromes which may be present in SLE, including focal manifestations (e.g. stroke or seizure) and diffuse syndromes (e.g. depression, anxiety, memory deficits, and general cognitive decline). The focal presentations of NPSLE, which are fairly well understood, are most frequently associated with autoantibodies that cause a hypercoagulable state, such as anti-phospholipid, anti-cardiolipin, and lupus anticoagulant antibodies[7]. At least twenty lupus autoantibodies have been found with correlation to NPSLE especially in the serum and cerebrospinal fluid (CSF) of patients such as anti-nuclear antibody (ANA), anti-N-methyl-D-aspartate receptor, and more[8–11]. In addition, a variety of cytokines have been identified as inflammatory mediators which play a pathogenic role and might disrupt the Blood brain barrier (BBB) including IL-1, IL-6, IFNα and TNFα, and TNF-like weak inducer of apoptosis (TWEAK)[5,12,13]. While our understanding of autoimmune dynamics is quite advanced for certain manifestations of SLE, there remain many unanswered questions regarding the mechanisms underlying neuropsychiatric disease in SLE patients (NPSLE).

The discovery of circulating brain reactive lupus autoantibodies in patients and in mouse models highlighted their potential central nervous system (CNS) pathogenicity[8]. Introducing anti-N-methyl-D-aspartate receptor antibodies (anti-NMDAR) directly into the brains of non-autoimmune mice was found to induce neuronal cell death and impair cognition[9,14], and these have been found in the CSF of SLE patients with CNS disease[8]. Consequently, neuropathic autoantibodies, including anti-NMDAR[4] and anti-ribosomal-P[15], are suggested to be effectors of NPSLE. These studies, however, also demonstrated that circulating neuropathic autoantibodies do not readily access the brain. Only with pharmacological breach of the blood-brain barrier (BBB), triggered by intravenous administration of lipopolysaccharide or epinephrine, may pathogenic autoantibodies access the brain to exert their neurotoxic effects[9].

The identification of such neuropathic autoantibodies in the CSF of SLE patients and in *post mortem* brains strongly supports brain penetrance[9]. While the exact route of antibody entry into the brain and solid evidence for NPSLE-related BBB disruption is missing, the prevalent working hypothesis is that abnormal permeabilization of the BBB is the primary contributor to neuropsychiatric disease in lupus. Nevertheless, abnormal antibody brain

penetrance might actually result from a dysfunction in any of the three brain barriers: the BBB, the meningeal barrier, or the blood-CSF barrier (BCSFB). Indeed, the involvement of brain barriers other then the BBB in the pathophysiology of lupus was previously proposed[5,16]. A convincing body of research supports this notion, including the following studies: First, the report of leptomeningeal abnormalities on Gd-DTPA (gadolinium) enhanced magnetic resonance (MRI) imaging that might reflect meningeal barrier abnormalities[17]. Second, elevated levels of albumin and antibodies found in the CSF of SLE patients might reflect BCSFB abnormalities[18,19]. Third, the presence of lymphoid cells in brain ventricles of NPSLE mouse models also led to the hypothesis that immune cells enter into the CSF and induce primary neuronal damage in regions bordering the cerebral ventricle[20]. Finally, CSF from both mice and humans with NPSLE is toxic for neurons and proliferating neural cells[21,22].

In our study we directly investigated the function of brain barriers in an established NPSLE mouse model, the MRL/MPJ-Fas^{lpr}/J mouse (hereafter MRL/lpr). Several spontaneous models of SLE with CNS manifestations exist, including NZB/W-F1, BXSB, and MRL/lpr mice[23,24]. Of these, the MRL/lpr mouse has proven to be a very useful spontaneous model of both SLE and NPSLE, for several reasons. Besides a strong female bias (similar to the human SLE 9:1 female to male ratio), the MRL/lpr mouse has a very similar overall disease pattern to human SLE including renal and cutaneous manifestations[25,26], as well as a neuropsychiatric profile consistent with the diffuse manifestations of human NPSLE including depression-like behavior and memory deficits[27,28]. Importantly, brain reactive lupus autoantibodies were found in both NPSLE patients and in this mouse model[8,29]. There is a significant and growing body of research into manifestations of NPSLE in MRL/lpr mice, including extensive behavioral characterization and brain tissue evaluation[28,29]. Therefore, here we utilized the MRL/lpr mouse strain to thoroughly investigate BBB integrity. Contrary to the commonly held view, exogenous tracer challenges (introducing different tracers into the blood circulation) with confocal and electron microscopy imaging showed no direct evidence of changes in BBB permeability. However, we report an unexpected mechanism of pathology, which likely represents the primary route of antibody entry into the brain through a perturbed BCSFB, a mechanism aligned with previous reports of choroid plexus and CSF antibody enrichment in NPSLE patients[18,19,30]. Based on our findings, we suggest a need to develop new avenues of research by shifting attention from BBB to BCSFB dysfunction.

2. Materials and Methods

2.1 Mice

8-week old female MRL/MPJ-*Fas*^{lpr}/J (stock #00485, (hereafter MRL/lpr)) and MRL/MPJ (stock #00486, hereafter MRL/+) mice were purchased from the Jackson Laboratories (Bar Harbor, ME) to establish a local colony. Pups were weaned at 3 weeks of age and raised until 5 or 16 weeks of age, as indicated in each experiment. All mice were bred and maintained in the animal facility of the Hebrew University under specific pathogen-free conditions. All animals were treated according to institutional guidelines approved by the Institutional Animal Care and Use Committee (IACUC) at Hebrew University.

2.2 Disease state evaluation

The MRL/lpr disease phenotype was scored in order to evaluate systemic disease progression as previously described[31]. In brief, phenotype evaluation included scoring of proteinuria (examined by CYBOW 10AC reagent strips for urinalysis)[32] and titers of IgG anti-double stranded (ds)DNA antibodies (examined by enzyme-linked immunosorbent assay (ELISA)[32].

2.3 Tissue preparation

After dissection, brains were placed in 4% paraformaldehyde (PFA, Sigma Aldrich) at 4°C overnight, cryopreserved in 30% sucrose and frozen in TissueTek OCT (Sakura). Frozen brains were cut to either 30 μm (for vessel profiling) or 10 μm slices for immunofluorescence staining (CM1950, Leica) to produce sagittal brain sections. In all experiments either cortex or choroid plexus (CP) were examined and analyzed[33,34].

2.4 Immunofluorescence

10μm thick cryo-sections were washed with phosphate buffered saline (PBS) for 15 min at room temperature (RT) and then incubated for 1 h at RT with blocking solution (10% bovine serum albumin (BSA), 10% normal horse serum (NHS), 0.05% triton X-100 in PBS). Slides were incubated with primary antibodies (diluted in 2.5% BSA, 2.5% NHS, 0.05% triton X-100 in PBS) at 4°C overnight. Slides were then washed with PBS, incubated with secondary antibodies for 1 h at RT, washed and mounted with 4',6-diamidino-2-phenylindole (DAPI) Fluoromount-G (Southern Biotech).

Primary antibodies used were: hamster anti-mouse CD31 (1:100, Bio-Rad cat No. MCA1370Z), and horseradish peroxidase (HRP)-donkey anti-mouse IgG (1:200 Southern Biotech cat No. 641005) and rabbit anti-albumin (1:200, sigma-Aldrich cat No.A0433).

Secondary antibodies used were: Cy3 donkey anti-mouse IgG (1:500, Jackson cat No. 715165151), goat anti-Armenian hamster (1:500, Jackson cat No.127605160) and Alexa 488 donkey anti-mouse IgG (1:200, Jackson cat No.715545151).

2.5 Leakage analysis

In all experiments, a leakage incident was defined when a tracer was localized outside the endothelial area. At least four non-sequential sagittal sections per animal (of similar cortical locations) were scanned under the microscope and analyzed by a person blind to the animal genotype.

2.5.1—IgG: 10 μm cryo-sections of 5 and 16-week old MRL/lpr and age-matched control MRL/+ mice were co-stained against CD31 and endogenous mouse IgG.

2.5.2—Dextran: Deeply anesthetized 5 and 16-week old MRL/lpr and age-matched control MRL/+ and age-matched control MRL/+ mice were injected transcardially with 1 mg/mL dextran, with volumes normalized to mice body weight (tetramethylrodamine, 10,000 MW, D 1817 Molecular Probes). The tracer was allowed to circulate for 5 min. Following

dissection and tissue preparation as described above, 10 μm cryo-sections were stained with hamster anti-mouse CD31.

2.5.3—IgG-HRP: Whole brains of 16-week old MRL/lpr mice were fixed with 2.5% gluteraldehyde, 2% PFA, 0.1 M $CaCO_2$ and 0.4% $CaCl_2$ for 1 h at RT and then for 3 h at 4°C. Brains were washed and left over night in 0.1 M $CaCO_2$ and 0.4% $CaCl_2$. 50 μm thick sections were prepared with a vibrotome (VT1000 S, Leica) and blocked overnight in 5% NHS serum solution. Slices were incubated with primary HRP anti-mouse antibody (1:500, Southern Biotech, 641005) for 48 h at 4°C followed by extensive washing. For 3,3′-Diaminobenzidine (DAB) staining, sections were incubated in 0.05 M Tris-HCl buffer (pH 7.6) containing 5 mg 3-3' diaminobenzidine (Thermo Scientific, TA-060-HDX) per 10 mL buffer and a final concentration of 0.01% hydrogen peroxide for 15 min at RT. The DAB reaction was stopped with PBS wash and quenched by post fixation in 2% osmium tetroxide sodium cacodylate buffer following by Transmission Electron microscopy (TEM) processing as described in 2.5. For bright field microscopy, sections were washed and post-fixed with 4% PFA for 15 min, washed and mounted.

2.5.4—HRP: Deeply anesthetized 16-week old MRL/lpr mice were injected with 0.4 mL of HRP (Sigma Aldrich, HRP type II, 10 mg/20 g mouse body weight, dissolved in PBS) through the tail vein. After 1 h of HRP circulation, brains were dissected and fixed by immersion in a 0.1 M sodium-cacodylate-buffered mixture (5% glutaraldehyde and 4% PFA) for 1 h at RT followed by 5 h in 4% PFA at 4 °C. Following fixation, the tissue was washed overnight in 0.1 M sodium-cacodylate buffer. 100 μm thick sections were prepared with a vibrotome, developed with DAB as described in 2.4.3 following by TEM processing as described in 2.5.

2.5.5—IgG-Rhodamine Red-X: Deeply anesthetized 16-week old MRL/lpr mice were injected with 1.5 mg/mL Rhodamine Red-X conjugated goat anti rabbit IgG (150 μg/20 g mouse body weight, Jackson Cat No. 111295144) through the tail vein and left circulating for 30–60 min. after circulation brains were dissected processed as described in the 2.2.

2.5.6—NHS-Biotin: Deeply anesthetized 16-week old MRL/lpr and age-matched control MRL/+ mice were perfused with 0.5 mg/mL sulfo-NHS-biotin (20 mL/30 g mouse body weight, Thermo Scientific, cat no. 21217, dissolved in PBS). Following 5 min perfusion with the tracer, mice were perfused with 2% PFA. Brains were dissected and placed in 4% PFA overnight. 100 μm sagittal sections were prepared with a vibrotome and were immunostained with streptavidin, and with anti-mouse CD31 and scanned with confocal microscope. Leakage incidents were defined in 3D projections of 100 μm sections (5 μm optical sections intervals).

2.5.7—Evans Blue - Evans Blue dye (2% in saline, 4 mL/kg mouse body weight, Sigma cat no. E-2129) was injected through the tail vein of 16-week old MRL/lpr mice and allowed to circulate for 5 mins. Deeply anesthetized mice were perfused with cold PBS for 15 min to remove the intravascular dye, following which dissection and tissue preparation was performed as described in the 2.2.

2.6 Transmission electron microscopy (TEM)

Freshly dissected tissue samples were fixed with Karnovsky's fixative (2% PFA, 2.5% glutaraldehyde in 0.1 M cacodylate buffer, pH=7.4) for 4 h at RT, followed by a 1:2 dilution of Karnovsky's fixative in 0.1 M cacodylate buffer overnight at 4°C. Samples were post-fixed in 1% $Os0_4$ in 0.1 M cacodylate buffer for 2 h, dehydrated in a graded series of alcohols, and embedded in epoxy resin. Sections of 60–80 nm were cut on an ultramicrotome (Ultracut, Reichert-Jung), contrasted with uranyl acetate and lead citrate, and examined with a Jeol (JEM-1400 PLUS, Japan) electron microscope.

2.7 Scanning electron microscopy (SEM)

Mice were transcardially perfused with ice cold PBS followed by a solution of ice-cold 2.5% glutaraldehyde with 0.1 M sodium cacodylate, 0.2 M sucrose, and 5 mM $MgCl_2$ pH 7.4. Brains were subsequently dissected and post-fixed for 72 h in the same fixative at 4°C, and sectioned with a Leica vibratome at 100 μm. Sections were dehydrated through a graded series of ethanols, critical point dried using liquid carbon dioxide in a Tousimis Samdri 795 Critical Point Drier (Rockville MD), and sputter coated with chromium in a Quorum EMS 150T ES (Quorum Technologies Ltd, United Kingdom). Sections were examined in a Zeiss supra field emission scanning electron microscope (Carl Zeiss Microscopy, LLC North America), using an accelerating voltage of 2 kV.

2.8 Fluorescence microscopy

Immunofluorescence images were captured using the following confocal microscopes: Nikon Eclipse Ni, objective ×20 and ×40 with Nikon C2 camera and Nis-Elements software, or with Nikon TE-2000, objective ×20, ×40 and ×60 with EZ-C1 software.

2.9 Statistics

Mann-Whitney U test (non-normally distributed data) was used for two-group comparisons, $p<0.05$ was considered significant.

3. Results

Evaluation of barrier function using imaging modalities (computerized tomography (CT) or MRI) in NPSLE patients has limited spatial resolution. Even if leakage can be identified, it is not likely to have sufficient specificity to ascertain which of the three brain barriers is dysfunctional (BBB, meningeal barrier, or BCSFB). Reliable and comprehensive evaluation of brain barrier function is, however, feasible in NPSLE mouse models[9].

3.1 Normal BBB permeability in the neuropsychiatric lupus mouse model

We evaluated BBB function in 16-week old MRL/lpr female mice, an age and sex by which systemic and neuropsychiatric disease phenotypes are pronounced (leading eventually to lethality). In all experiments, we compared these with age matched MRL/+ control mice, a parental congenic mouse strain in which an attenuated disease phenotype starts only very late and with no NPSLE phenotypes (life span is approximately 17 weeks in MRL/lpr females compared with approximately 73 weeks in MRL/+ females). Leakage quantification

focused on the cortex to avoid regions with a higher degree of physiological permeability (e.g. circumventricular organs). Key SLE disease phenotypes (proteinuria and anti-dsDNA antibody concentrations) were monitored to evaluate disease progression[31].

We evaluated the extravasation of endogenous tracers (serum proteins that normally do not cross the BBB), previously shown to abnormally extravasate across the MRL/lpr BBB[32,35]. Thin cortical sections were stained for CD31 (vascular labeling) together with staining for mouse IgG, and imaged with fluorescence microscopy. We found that BBB function of the overall vascular network was normal, effectively restricting IgG signal to the vessel lumen (Figure 1A, upper panel). In both NPSLE and control mice IgG leakage was relatively uncommon and mostly deposited in parenchyma surrounding medium or large size vessels (Figure 1A). Quantification revealed that such leakage was uncommon in the cortex (at most, 1–2 events per cortical slice) and did not significantly differ between genotypes (Figure 1B). An average of 0.25±0.08 (mean ± s.e.m) and of 0.25±0.11(mean ± s.e.m) leakage incidents per slice appeared in in MRL/lpr and MRL/+ sections, respectively.

We next used exogenous tracer challenges (a more potent leakage test), intracardially injecting MRL/lpr and control MRL/+ mice with 10 kDa rhodamine-dextran for acute tracer challenges. Again, the BBB functioned normally (Figure 1C), and the prevalence of leakage did not significantly differ between genotypes (Figure 1D). An average of 0.2±0.13 (mean ± s.e.m) and of 0.14±0.09 (mean ± s.e.m) leakage incidents per slice appeared in MRL/lpr and MRL/+ sections respectively.

To exclude the possibility that we overlooked possible changes in barrier selectivity, we tested barrier permeability to various tracers of different molecular size and composition. We used endogenous tracers, including staining for albumin (data not shown) and a different imaging approach for endogenous IgG (chromogenic HRP imaging; Supplementary Figure 1A). We employed additional exogenous tracers, including ~443 Da biotin and Evans blue (960 Da tracer, reflecting albumin-dye complexes of approximately 65kDa, data not shown), ~160kDa rhodamine-red-X conjugated goat IgG (Supplementary Figure 1B) and ~44kDa horseradish peroxidase (HRP, Figure 1E). Results of all six additional tracer experiments indicated a normally functional and selective BBB. Moreover, preserved BBB function was present despite concurrent development of significant indicators of systemic disease in these same MRL/lpr mice, including high titers of anti-dsDNA antibodies and significant proteinuria (data not shown). Finally, normal BBB function was observed in 5-week old MRL/lpr mice, before an overt NPSLE phenotype is evident (Supplementary Figure 1C), thereby excluding the possibility that an early BBB dysfunction might be a contributing factor of NSPLE.

3.2 BBB endothelium of NPSLE mice exhibits normal ultrastructure and function of cellular selectivity features

TEM imaging of the BBB ultrastructure revealed no evidence of changes in cell structure that could support BBB endothelial selectivity abnormalities such as tight junction distortions or hyper-vesicular activity (Figure 1E). Moreover, we could demonstrate that NPSLE BBB endothelial cell selectivity features functioned normally. Using exogenous HRP tracer challenges we examined the function of tight junctions and transcytosis with

TEM imaging. Neither luminal and abluminal plasma membranes invaginations, nor cytoplasmic vesicles had any signs of tracer loading/transport, excluding the possibility of abnormal upregulation of the transcytotic pathway (Figure 1E). Ample tracer could be found in capillary lumens advancing toward junctional structures, stopping at the luminal portion of the tight junction, never penetrating into the brain side (Figure 1E, arrow). We could not detect any evidence of tracer at the basement membrane. Altogether, based on our thorough investigation of BBB function and structure, we concluded that antibody penetration into the brain of NPSLE mice most probably does not frequently occur through a dysfunctional BBB.

3.3 The neuropsychiatric lupus mouse model exhibits irregular IgG deposits at sub ventricular zones

Taking into consideration previous reports of CSF containing antibodies in this neuropsychiatric lupus mouse model together with our data indicating a normal BBB, we hypothesized that there should be an alternative route of antibody entry into the CNS. Examining IgG staining of 16-week old MRL/lpr female mice brain sections, we noticed irregular periventricular IgG deposits, which were absent from control MRL/+ brain sections (Figure 2). IgG was found covering the ependymal layer and also present in brain parenchyma of sub ventricular zones at lateral, 3rd and 4th brain ventricles. Two possible routes of abnormal IgG leakage into the sub-ventricular zone might be considered: the first is through the BBB of parenchymal capillaries residing within the sub-ventricular zone and the second is through a dysfunctional BCSFB. The later would involve the following path: Antibodies normally extravasate from the blood through fenestrated capillaries of the choroid plexus (CP) into the CP stroma. From there antibodies might abnormally cross the BCSFB (a single layer of CP epithelium) into the CSF. Ependymal cells lining ventricle walls function as a CSF-brain barrier only during embryonic development, but are readily permeable in adults[36]. Thus, if the BCSFB is dysfunctional, allowing antibody leakage from the blood into the CSF, they could accumulate in periventricular regions. Indeed, using imaging of endogenous IgG with chromogenic HRP reactions we could demonstrate as expected IgG in CP vessels and CP stroma (Supplementary Figure 2, arrow) but also in the sub ventricular zones, beyond the ependymal cell layer (Supplementary Figure 2, asterisks). A gradient of IgG staining appeared stronger at the ependymal layer, diminishing toward the brain parenchyma. This pattern might reflect IgG origins at the CSF.

3.4 Evidence of BCSFB dysfunction points to an alternative route of antibody entry into the CNS at the choroid plexus

The choroid plexus is an epithelial bilayer surrounding a highly vascularized capillary plexus. This epithelium synthesizes CSF but also separates brain ventricles from the blood, forming the BCSFB (Figure 3A, illustration). In both NPSLE patients and mouse models, the increase in albumin quotient (Qalb), measured by comparing the ratio of CSF to serum albumin, purportedly reflects BBB leakage[5], though likely is a better indicator of BCSFB leakage, given the sampled substrate. We therefore sought direct evidence of abnormal IgG passage across the BCSFB, by staining for IgG and closely examining the CP with confocal microscopy. In control MRL/+ CP sections, IgG was apparent only within the CP blood vessels and stroma (Figure 3B upper panel).

In contrast, in MRL/lpr CP sections, IgG could be detected also at the apical portion of the epithelium (Figure 3B middle and lower panels). In normal homeostatic conditions, the BCSFB is expected to exclude antibodies from the CSF. Abnormal localization of IgG at the ventricular side of the BCSFB might suggest barrier dysfunction. In order to gain higher resolution at the IgG localization we performed staining for IgG with HRP conjugated antibodies. Developing these sections with DAB allows detecting the IgG with TEM imaging (Figure 3C). With TEM, we could demonstrate the entire ventricular surface of the CP epithelium (epithelial microvilli) covered by IgG deposits (Figure 3C, left panel). We could not find clear evidence of vesicular IgG trafficking through the CP epithelium (transcytosis), but could show ample IgG deposition in the lateral labyrinth and basal faces of the epithelium (Figure 3C, right panel). Since both the HRP-DAB reaction products and tight junctions are electron dense, it is hard to determine whether IgG passage through junctions is occurring.

3.5 BCSFB dysfunction involves normal function of tight junctions but possible elevation of vesicular activity

Exogenous tracers are often used to identify mechanisms of barrier dysfunction (especially of the BBB). Challenging the BCSFB with exogenous tracers is not practical because leakage of tracers into the CSF is expected to rapidly defuse, making it hard to use imaging to identify changes in barrier properties. To circumvent this technical problem we used HRP as a tracer and imaged the BCSFB of MRL/lpr mice with TEM (Figure 4). HRP was injected into the blood stream followed by half an hour circulating time. Ample HRP could be detected inside CP vasculature, crossing the vasculature basement membrane and filling CP stroma (Figure 4B). Intracellular spaces between epithelial cells (lateral labyrinth) were also filled with HRP reaching the level of tight junctions. Nevertheless, we could not detect any evidence of tracer penetrating through tight junctions into the CSF compartment (Figure 4B, left). In contrast, we could detect epithelial cells with elevated vesicular activity (Figure 4C). HRP filled vesicles were found in epithelial cells, mostly in the basal portion of the cells. It seemed that not all epithelial cells were affected and we could not find evidence of HRP loaded vesicles fusing with the apical membrane. Taken together, we could exclude the possibility of abnormal junctional transport, and conclude that elevated transcytosis might be the mechanism of barrier dysfunction (Figure 4A, illustration).

3.6 The primary site of leukocyte entry into the brain in NPSLE likely occurs at the choroid plexus

Another fundamental property of brain barriers is their ability to sequester the CNS from immune cell entry. The majority of studies examining immune cell infiltration into the brains of MRL/lpr mice documented T cell entry[37]. Intrathecal antibody production, indicating the presence of plasma cells in brain parenchyma, was also suggested, but all brain regions identified as sites of plasma cell localization were regions adjacent to ventricles or meninges, including the stria medullaris and interhemispheric fissure[37]. In contrast to the modest infiltration into brain parenchyma itself, we and others have reported robust cellular infiltration into the choroid plexus stroma of MRL/lpr mice, including the presence of plasma cells[5]. This infiltration has been previously characterized as mixed in nature, but

elsewhere we present evidence supporting the formation of organized tertiary lymphoid structures within the CP[38].

Extensive CP infiltration has the potential to induce disruption of BCSFB properties facilitating abnormal immune cell passage and changes in barrier permeability to certain molecules such as antibodies, cytokines, solutes, etc. Indeed, we noticed that the presence of IgG at the ventricular side of the BCSFB was more common in CP regions where immune cells infiltrated the stroma (Figure 3B lower panel represents highly infiltrated regions, Figure 3B middle panel represents less infiltrated regions).

Under homeostatic conditions, the CP barrier facilitates lymphocyte passage into the ventricle under interferon-γ regulation[39,40]. Supporting such a transport route in NPSLE, elsewhere we also report up-regulation of a CP interferogenic expression signature in MRL/lpr mice[38]. Nevertheless, if and how immune cells penetrate the brain compartment (i.e the CSF) across the BCSFB in NPSLE is less clear. To investigate this possibility, we imaged the CP with SEM. Lymphocytes, both dispersed and in groups, localized to the ventricular surface of the epithelium were more abundant in MRL/lpr than in MRL/+ CP (Figure 5A). Passage of lymphocytes through the BCSFB likely occurs through trans-epithelial migration as indicated by TEM imaging displaying lymphocyte localization along the expected pathway - lymphocytes are found inside CP vessels, and between the vessel's basement membrane and the epithelium basement membrane (Figure 5B, upper panel). We could often identify lymphocytes engulfed by epithelial cells (Figure 5B, upper panel) and also at the apical/ventricular side of the epithelium (Figure 5B, lower panels). We also noticed many lymphocytes occupying baso-lateral spaces adjacent to epithelial adherence junctions but could not identify lymphocytes crossing through tight junctions.

We conclude therefore that the CP epithelial barrier is compromised in MRL/lpr mice, as shown by abnormal IgG leakage and by abundant trans-epithelial passage of immune cells.

4. Discussion

The results from our tracer experiments challenge the commonly held view of BBB disruption in NPSLE, at least with regards to the prevalently utilized mouse model, with only relatively minor leakage observed. The uncommon leakage incidents, which were restricted to medium-large vessels, might indicate some specific disruption at the level of arterioles or venules. This, however, may be a feature of the genetic background, since it appeared in the control mice as well. These isolated incidents may not represent leakage across the BBB but rather leakage into the CSF that could be then concentrated in the perivascular space around medium sized vessels, bounded by the astrocytic end-feet, along the track of the "glymphatic" system[41].

We describe here an alternative route of antibody entry into the brain of NPSLE mice through the BCSFB. While neuropathic autoantibodies are suggested to be effectors of NPSLE[15,42], additional studies will be required in order to confirm the contribution of BCSFB disruption to the pathogenesis of NPSLE. Indications of the clinical relevance of this alternative route in human NPSLE includes reports of proteinaceous deposits within the

CP basement membrane[43–45] and MRI imaging studies demonstrating periventricular white matter hyperintensities that may correlate with these regions being affected by BCSFB dysfunction[46]. Moreover, based on our study we suggest considering that previous data from both NPSLE patients and mouse models showing an increased albumin quotient (Qalb) and IgG index[5] reflects BCSFB rather than BBB leakage.

Local antibody production by plasma cells in CP stroma, which juxtaposes the epithelium, makes the CP a plausible source and the CSF a sink for antibodies, with immediate passage through a compromised epithelial barrier. At this time we cannot exclude the possibility that the source of IgG covering the ventricular surface of the epithelium are plasma cells residing in the CSF compartment. In fact our EM imaging data of lymphocytes on the ventricular surface of the epithelium and along the trans-epithelial pathway warrant the need for future investigation of abnormal B cells/plasma cells passage. In this respect, our study joins previous reports of other pathologies such as multiple sclerosis (mainly findings from experimental autoimmune encephalomyelitis (EAE) mouse models[47–49]) and also a recent study on stroke, identifying the CP as a key cerebral invasion route for T cells[50].

Previous reports of BCSFB trans-epithelial migration during inflamed CP conditions suggested changes in immune adhesion molecule localization[20]. Seeking molecular evidence to support changes in barrier properties, we isolated CP from MRL/lpr and MRL/+ mice and examined levels of mRNA with real time PCR for immune adhesion genes (VCAM and I-CAM-1) and for epithelial specific structural tight junction genes (Claudin 2, JAM 2, JAM 3, ZO 1–3, and Cadherin 23). We could not find significant changes in mRNA levels of these candidate genes (data not shown). Epithelial cell isolation with an unbiased, whole genome analysis approach could better help evaluating such molecular changes in future studies.

Regarding changes in barrier permeability, our data support up-regulation of transcytosis rather than of junctional transport. Elevated vesicular activity could mediate IgG transport across the BCSFB in transcytotic vesicles. Previous studies have demonstrated the expression of the neonatal Fc receptor (FcRn) in adult brain endothelial cells and in the ependymal cells of the choroid plexus[51]. This receptor is known to mediate transcytosis of IgG (as well as of albumin) from the mother to the fetus across the placenta barrier. A process of reverse IgG transport from the CSF via the BCSFB epithelium into the blood, or reverse IgG transport from the brain parenchyma via BBB endothelium into the blood, was suggested based on rapid efflux of IgG that was injected into the brain[52]. Antibodies with high affinity to FcRn are cleared faster once injected into the brain than these with low affinity, indicating its possible function in clearing antibodies from the brain[53]. On the other hand, studies of knockout mice lacking FcRn do not support a role for FcRn in reverse transcytosis[54]. It would be interesting to test the possibility that FcRn function, localization, or expression levels are changed at the BCSFB in NPSLE. This in turn might influence either the clearance of IgG from the CSF or the abnormal import of IgG across this barrier.

Another possible mechanism could be that IgG occupies macro-pinocytosis vesicles created when epithelial cells engulf lymphocytes. Indeed we found evidence for such events when examining lymphocyte crossings in the CP of HRP injected mice. Finally, TEM profiles of lymphocytes did not resemble typical plasma cells but might include B cells. The fact that

endogenous IgG is found in the apical side of the epithelium while exogenous challenges with HRP failed to exhibit similar localization might support local production of IgG in the CSF. On the other hand, exogenous challenges with HRP might be too short to allow robust passage of this tracer.

BCSFB disruption would allow abnormal CNS exposure to neuropathic autoantibodies. Periventricular brain regions are expected to be the immediate affected regions, but taking into account that CSF intermixes with interstitial brain fluids through the “glymphatic” system[41], BCSFB disruption is also expected to allow exposure of the entire brain parenchyma to neuropathic autoantibodies.

5. Conclusions

In our study we examined BBB integrity in an established NPSLE mouse model. Surprisingly, we found that the BBB is not majorly perturbed. In contrast, we found that blood-CSF barrier dysfunction facilitates both brain exposure to antibodies and abnormal lymphocyte entry into ventricles. Our results challenge the commonly held view of BBB disruption, and support a shift in focus to BCSFB dysfunction as a causative factor in NPSLE. This new focus could hopefully lead to new avenues of research, and eventually the development of specific therapies for restoring BCSFB function.

Supplementary Material

Refer to Web version on PubMed Central for supplementary material.

Acknowledgments

We thank the electron microscopy intra-departmental core facility at the Hebrew University Faculty of Medicine, and the analytical imaging facility at the Albert Einstein College of Medicine, for technical support and valuable scientific advice. We thank Dr. Gillian Kay for valuable scientific editing.

Funding

These studies were supported by research grants from the Abisch-Frenkel Foundation (15/H1) and the Leona M. and Harry B. Helmsley Charitable Trust (2015PG-ISL007) to A. Ben-Zvi; a RO1 grant from the National Institute of Arthritis and Musculoskeletal Diseases (AR065594) to C. Putterman; and training grant T32-GM007288 to A. Stock from the NIH.

References

1. Tsokos GC. Systemic lupus erythematosus. N Engl J Med. 2011; 365:2110–2121. DOI: 10.1056/NEJMra1100359 [PubMed: 22129255]
2. Lisnevskaia L, Murphy G, Isenberg D. Systemic lupus erythematosus. Lancet. 2014; 384:1878–1888. DOI: 10.1016/S0140-6736(14)60128-8 [PubMed: 24881804]
3. Mok CC, Lau CS. Pathogenesis of systemic lupus erythematosus. J Clin Pathol. 2003; 56:481–490. [PubMed: 12835292]
4. Popescu A, Kao AH. Neuropsychiatric systemic lupus erythematosus. Curr Neuropharmacol. 2011; 9:449–457. DOI: 10.2174/157015911796557984 [PubMed: 22379459]
5. Stock AD, Gelb S, Pasternak O, Ben-Zvi A, Putterman C. The blood brain barrier and neuropsychiatric lupus: new perspectives in light of advances in understanding the neuroimmune interface. Autoimmun Rev. 2017; 16:612–619. DOI: 10.1016/j.autrev.2017.04.008 [PubMed: 28428121]

6. Gulinello M, Wen J, Putterman C. Neuropsychiatric Symptoms in Lupus. Psychiatr Ann. 2012; 42:322–328. DOI: 10.3928/00485713-20120906-05 [PubMed: 25620816]
7. Devreese KM. Standardization of antiphospholipid antibody assays. Where do we stand? Lupus. 2012; 21:718–721. DOI: 10.1177/0961203312439335 [PubMed: 22635211]
8. DeGiorgio LA, et al. A subset of lupus anti-DNA antibodies cross-reacts with the NR2 glutamate receptor in systemic lupus erythematosus. Nat Med. 2001; 7:1189–1193. DOI: 10.1038/nm1101-1189 [PubMed: 11689882]
9. Kowal C, et al. Human lupus autoantibodies against NMDA receptors mediate cognitive impairment. Proc Natl Acad Sci U S A. 2006; 103:19854–19859. DOI: 10.1073/pnas.0608397104 [PubMed: 17170137]
10. Faust TW, et al. Neurotoxic lupus autoantibodies alter brain function through two distinct mechanisms. Proc Natl Acad Sci U S A. 2010; 107:18569–18574. DOI: 10.1073/pnas.1006980107 [PubMed: 20921396]
11. Rekvig OP, et al. Autoantibodies in lupus: culprits or passive bystanders? Autoimmun Rev. 2012; 11:596–603. DOI: 10.1016/j.autrev.2011.10.021 [PubMed: 22041579]
12. Kivity S, Agmon-Levin N, Zandman-Goddard G, Chapman J, Shoenfeld Y. Neuropsychiatric lupus: a mosaic of clinical presentations. BMC Med. 2015; 13:43. [PubMed: 25858312]
13. Wen J, et al. TNF-like weak inducer of apoptosis promotes blood brain barrier disruption and increases neuronal cell death in MRL/lpr mice. J Autoimmun. 2015; 60:40–50. DOI: 10.1016/j.jaut.2015.03.005 [PubMed: 25911200]
14. Hirohata S, Arinuma Y, Yanagida T, Yoshio T. Blood-brain barrier damages and intrathecal synthesis of anti-N-methyl-D-aspartate receptor NR2 antibodies in diffuse psychiatric/neuropsychological syndromes in systemic lupus erythematosus. Arthritis Res Ther. 2014; 16:R77. [PubMed: 24655341]
15. Yoshio T, Hirata D, Onda K, Nara H, Minota S. Antiribosomal P protein antibodies in cerebrospinal fluid are associated with neuropsychiatric systemic lupus erythematosus. J Rheumatol. 2005; 32:34–39. [PubMed: 15630721]
16. Abbott NJ, Mendonca LL, Dolman DE. The blood-brain barrier in systemic lupus erythematosus. Lupus. 2003; 12:908–915. [PubMed: 14714910]
17. Okano R, Kuroki M, Otsuka M, Yamada A, Ueki A. Leptomeningeal abnormality on Gd-DTPA enhanced MRI in a case of SLE presenting diffuse organic brain syndrome. Rinsho Shinkeigaku. 1993; 33:78–82. [PubMed: 8334780]
18. Ganrot K, Laurell CB. Measurement of IgG and albumin content of cerebrospinal fluid, and its interpretation. Clin Chem. 1974; 20:571–573. [PubMed: 4207912]
19. Ho RC, et al. A meta-analysis of serum and cerebrospinal fluid autoantibodies in neuropsychiatric systemic lupus erythematosus. Autoimmun Rev. 2016; 15:124–138. DOI: 10.1016/j.autrev.2015.10.003 [PubMed: 26497108]
20. Sakic B, et al. Increased TUNEL staining in brains of autoimmune Fas-deficient mice. J Neuroimmunol. 2000; 104:147–154. [PubMed: 10713354]
21. Maric D, et al. Neurotoxic properties of cerebrospinal fluid from behaviorally impaired autoimmune mice. Brain Res. 2001; 920:183–193. [PubMed: 11716824]
22. Sakic B, et al. Proliferating brain cells are a target of neurotoxic CSF in systemic autoimmune disease. J Neuroimmunol. 2005; 169:68–85. DOI: 10.1016/j.jneuroim.2005.08.010 [PubMed: 16198428]
23. Arabo A, Costa O, Dubois M, Tron F, Caston J. Effects of systemic lupus erythematosus on spatial cognition and cerebral regional metabolic reactivity in BxSB lupus-prone mice. Neuroscience. 2005; 135:691–702. DOI: 10.1016/j.neuroscience.2005.06.069 [PubMed: 16125863]
24. Vogelweid CM, Wright DC, Johnson JC, Hewett JE, Walker SE. Evaluation of memory, learning ability, and clinical neurologic function in pathogen-free mice with systemic lupus erythematosus. Arthritis Rheum. 1994; 37:889–897. [PubMed: 8003061]
25. Doerner JL, et al. TWEAK/Fn14 Signaling Involvement in the Pathogenesis of Cutaneous Disease in the MRL/lpr Model of Spontaneous Lupus. J Invest Dermatol. 2015; 135:1986–1995. DOI: 10.1038/jid.2015.124 [PubMed: 25826425]

26. Chalmers SA, et al. CSF-1R inhibition attenuates renal and neuropsychiatric disease in murine lupus. Clin Immunol. 2017; 185:100–108. DOI: 10.1016/j.clim.2016.08.019 [PubMed: 27570219]
27. Sakic B. The MRL model: an invaluable tool in studies of autoimmunity-brain interactions. Methods Mol Biol. 2012; 934:277–299. DOI: 10.1007/978-1-62703-071-7_14 [PubMed: 22933151]
28. Gulinello M, Putterman C. The MRL/lpr mouse strain as a model for neuropsychiatric systemic lupus erythematosus. J Biomed Biotechnol. 2011; 2011:207504. [PubMed: 21331367]
29. Gao HX, et al. Depression is an early disease manifestation in lupus-prone MRL/lpr mice. J Neuroimmunol. 2009; 207:45–56. DOI: 10.1016/j.jneuroim.2008.11.009 [PubMed: 19121871]
30. McLean BN, Miller D, Thompson EJ. Oligoclonal banding of IgG in CSF, blood-brain barrier function, and MRI findings in patients with sarcoidosis, systemic lupus erythematosus, and Behcet's disease involving the nervous system. J Neurol Neurosurg Psychiatry. 1995; 58:548–554. [PubMed: 7745401]
31. Deocharan B, et al. Alpha-actinin immunization elicits anti-chromatin autoimmunity in nonautoimmune mice. J Immunol. 2007; 179:1313–1321. [PubMed: 17617624]
32. Stock AD, et al. Neuropsychiatric systemic lupus erythematosus persists despite attenuation of systemic disease in MRL/lpr mice. J Neuroinflammation. 2015; 12:205. [PubMed: 26546449]
33. Ben-Zvi A, et al. Mfsd2a is critical for the formation and function of the blood-brain barrier. Nature. 2014; 509:507–511. DOI: 10.1038/nature13324 [PubMed: 24828040]
34. Lacoste B, et al. Sensory-related neural activity regulates the structure of vascular networks in the cerebral cortex. Neuron. 2014; 83:1117–1130. DOI: 10.1016/j.neuron.2014.07.034 [PubMed: 25155955]
35. Wen J, et al. B cell and/or autoantibody deficiency do not prevent neuropsychiatric disease in murine systemic lupus erythematosus. J Neuroinflammation. 2016; 13:73. [PubMed: 27055816]
36. Whish S, et al. The inner CSF-brain barrier: developmentally controlled access to the brain via intercellular junctions. Front Neurosci. 2015; 9:16. [PubMed: 25729345]
37. Ma X, Foster J, Sakic B. Distribution and prevalence of leukocyte phenotypes in brains of lupus-prone mice. J Neuroimmunol. 2006; 179:26–36. DOI: 10.1016/j.jneuroim.2006.06.023 [PubMed: 16904195]
38. 2017 ACR/ARHP Annual Meeting Abstract Supplement. Arthritis Rheumatol. 2017; 69(Suppl 10): 1–4426. DOI: 10.1002/art.40321
39. Kunis G, Baruch K, Miller O, Schwartz M. Immunization with a Myelin-Derived Antigen Activates the Brain's Choroid Plexus for Recruitment of Immunoregulatory Cells to the CNS and Attenuates Disease Progression in a Mouse Model of ALS. J Neurosci. 2015; 35:6381–6393. DOI: 10.1523/JNEUROSCI.3644-14.2015 [PubMed: 25904790]
40. Kunis G, et al. IFN-gamma-dependent activation of the brain's choroid plexus for CNS immune surveillance and repair. Brain. 2013; 136:3427–3440. DOI: 10.1093/brain/awt259 [PubMed: 24088808]
41. Yang L, et al. Evaluating glymphatic pathway function utilizing clinically relevant intrathecal infusion of CSF tracer. Journal of translational medicine. 2013; 11:107. [PubMed: 23635358]
42. Steup-Beekman G, Steens S, van Buchem M, Huizinga T. Anti-NMDA receptor autoantibodies in patients with systemic lupus erythematosus and their first-degree relatives. Lupus. 2007; 16:329–334. DOI: 10.1177/0961203307078224 [PubMed: 17576734]
43. Atkins CJ, Kondon JJ, Quismorio FP, Friou GJ. The choroid plexus in systemic lupus erythematosus. Ann Intern Med. 1972; 76:65–72. [PubMed: 4553744]
44. Sher JH, Pertschuk LP. Immunoglobulin G deposits in the choroid plexus of a child with systemic lupus erythematosus. The Journal of pediatrics. 1974; 85:385–387. [PubMed: 4610421]
45. Gershwin ME, Hyman LR, Steinberg AD. The choroid plexus in CNS involvement of systemic lupus erythematosus. The Journal of pediatrics. 1975; 87:588–590. [PubMed: 1159591]
46. Luyendijk J, et al. Neuropsychiatric systemic lupus erythematosus: lessons learned from magnetic resonance imaging. Arthritis Rheum. 2011; 63:722–732. DOI: 10.1002/art.30157 [PubMed: 21360502]

47. Wolburg K, Gerhardt H, Schulz M, Wolburg H, Engelhardt B. Ultrastructural localization of adhesion molecules in the healthy and inflamed choroid plexus of the mouse. Cell Tissue Res. 1999; 296:259–269. [PubMed: 10382270]

48. Engelhardt B, Ransohoff RM. Capture, crawl, cross: the T cell code to breach the blood-brain barriers. Trends Immunol. 2012; 33:579–589. DOI: 10.1016/j.it.2012.07.004 [PubMed: 22926201]

49. Schulz M, Engelhardt B. The circumventricular organs participate in the immunopathogenesis of experimental autoimmune encephalomyelitis. Cerebrospinal Fluid Res. 2005; 2:8. [PubMed: 16197544]

50. Llovera G, et al. The choroid plexus is a key cerebral invasion route for T cells after stroke. Acta Neuropathol. 2017; 134:851–868. DOI: 10.1007/s00401-017-1758-y [PubMed: 28762187]

51. Schlachetzki F, Zhu C, Pardridge WM. Expression of the neonatal Fc receptor (FcRn) at the blood-brain barrier. J Neurochem. 2002; 81:203–206. [PubMed: 12067234]

52. Zhang Y, Pardridge WM. Mediated efflux of IgG molecules from brain to blood across the blood-brain barrier. J Neuroimmunol. 2001; 114:168–172. [PubMed: 11240028]

53. Cooper PR, et al. Efflux of monoclonal antibodies from rat brain by neonatal Fc receptor, FcRn. Brain Res. 2013; 1534:13–21. DOI: 10.1016/j.brainres.2013.08.035 [PubMed: 23978455]

54. Garg A, Balthasar JP. Investigation of the influence of FcRn on the distribution of IgG to the brain. AAPS J. 2009; 11:553–557. DOI: 10.1208/s12248-009-9129-9 [PubMed: 19636712]

Highlights

1. The blood-brain barrier is not perturbed in neuropsychiatric lupus.
2. Blood-CSF barrier dysfunction facilitates brain exposure to antibodies.
3. Blood-CSF barrier facilitates abnormal lymphocyte entry into ventricles.

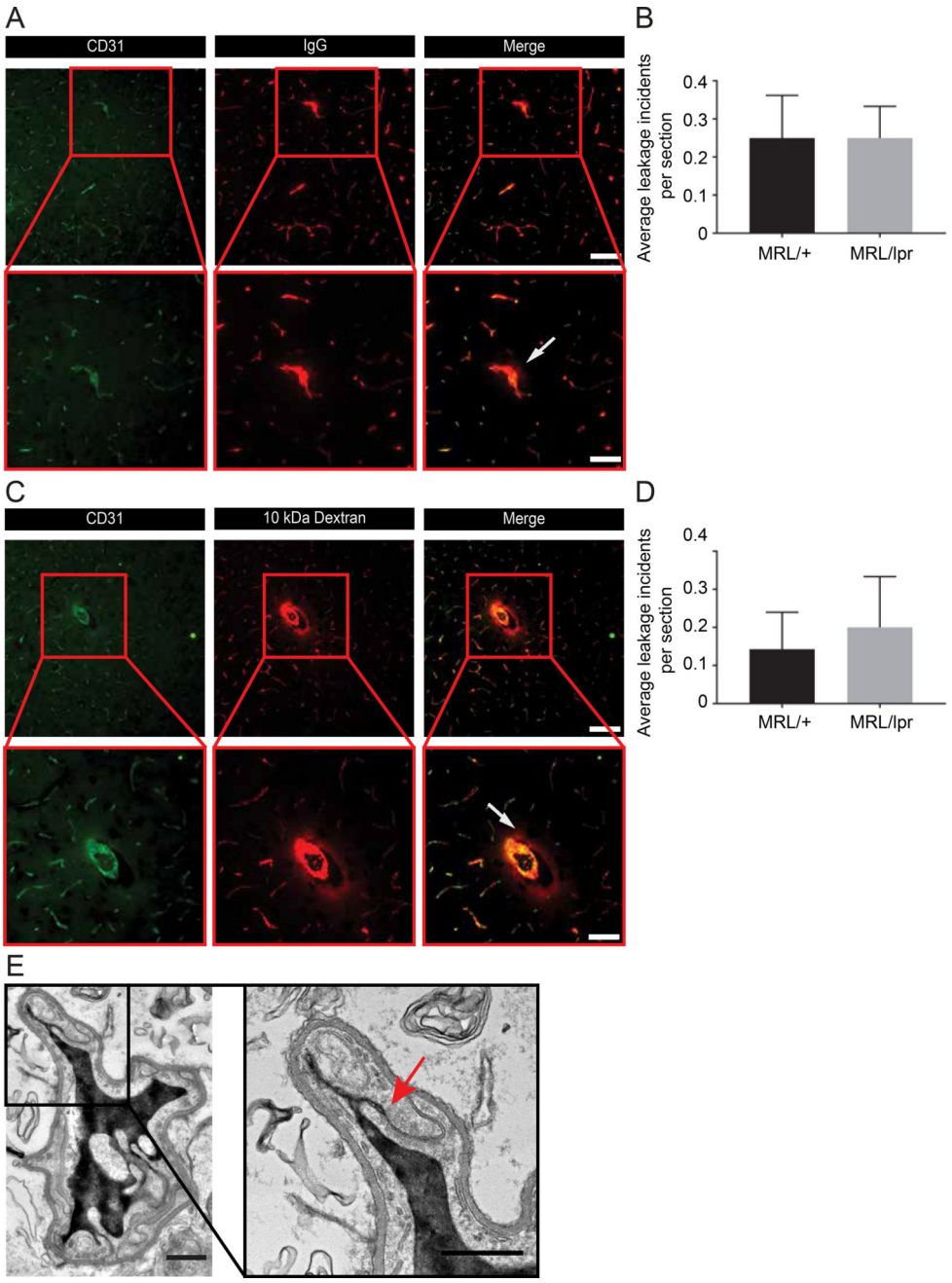

Figure 1. Blood-brain barrier permeability is preserved in NPSLE mice

Staining for endogenous intravascular proteins or following exogenous tracer challenges showed no indication of BBB hyper-permeability correlating with NPSLE progression. A. Female MRL/lpr mice (at 16 weeks of age, when active systemic and NPSLE manifestations are prevalent) and age-matched congenic control MRL/+ mice were co-stained for CD31 and for mouse IgG. B. Quantification shows that the prevalence of infrequent leakage incidents did not significantly differ between genotypes ($P>0.9$ as determined by a non-parametric Mann-Whitney U test). Leakage was defined as present when IgG was localized outside the endothelial area (outlined by the CD31 staining). At least four non-sequential

sagittal sections per animal were scanned under the microscope, and analyzed by an individual blinded to the animal genotype. C. MRL/lpr and control MRL/+ mice (at 16 weeks of age) were injected with 10 kDa rhodamine-dextran for short-term (5–10 min) tracer challenges and co-stained for CD31. D. Quantification shows that the prevalence of rare leakage incidents did not significantly differ between genotypes ($P>0.9$ as determined by a non-parametric Mann-Whitney U test). In both assays (A and C), fluorescence imaging was performed on cortical sagittal sections (covering visual and somatosensory regions of the cerebral cortex). BBB function of the overall vascular network was generally preserved, and the tracer signal restricted to the vessel lumen (upper panels). In both lupus and control mice, tracer leakage was relatively uncommon, and mostly restricted to parenchymal tissue surrounding medium-large size vessels (arrows, insets in lower panels). Images from MRL/lpr mice are representative of both genotypes. N=5 mice per group; for quantifications 10–24 sections per mouse were evaluated, scale bars 50 μm upper panels & 100 μm lower panels. E. TEM imaging of cortical capillaries from HRP injected, 16 week old female MRL/lpr mice. Capillary lumen is filled with HRP. No tracer leakage found demonstrating a functional tight junction (arrow) and no evidence of transcytosis. N=5 mice; scale bar 0.5 μm. All data are mean ± s.e.m.

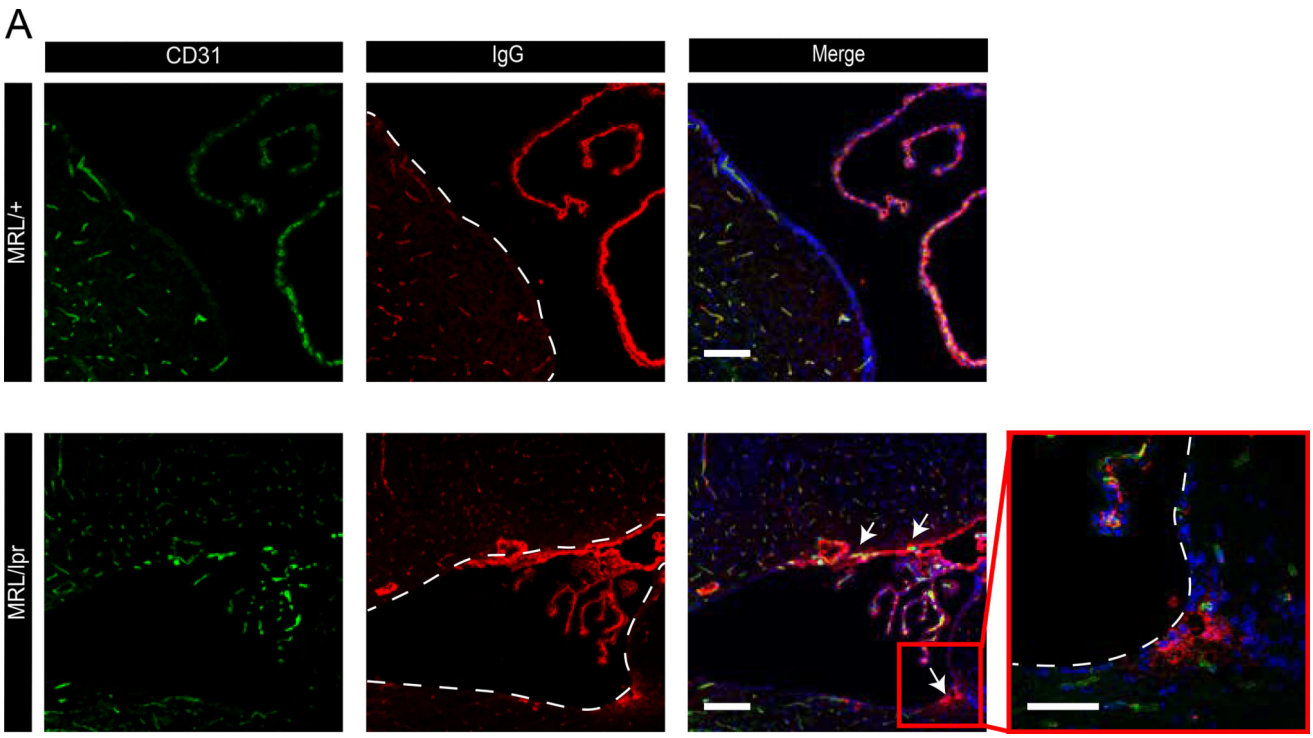

Figure 2. NPSLE mice exhibit IgG deposits at sub ventricular zones

Confocal imaging of 16 week old MRL/lpr mice brains co-stained for CD31 and for endogenous IgG, revealed irregular IgG deposits at sub ventricular zones (lower panel, ventricle bounders are indicated with dashed lines, aligned with ependymal cell layer. Arrows indicating sites of IgG deposits). IgG deposits were not found in control MRL/+ mice (upper panel). N=5 mice per group; scale bars 20 μm. Images taken from 10 μm brain sagittal sections.

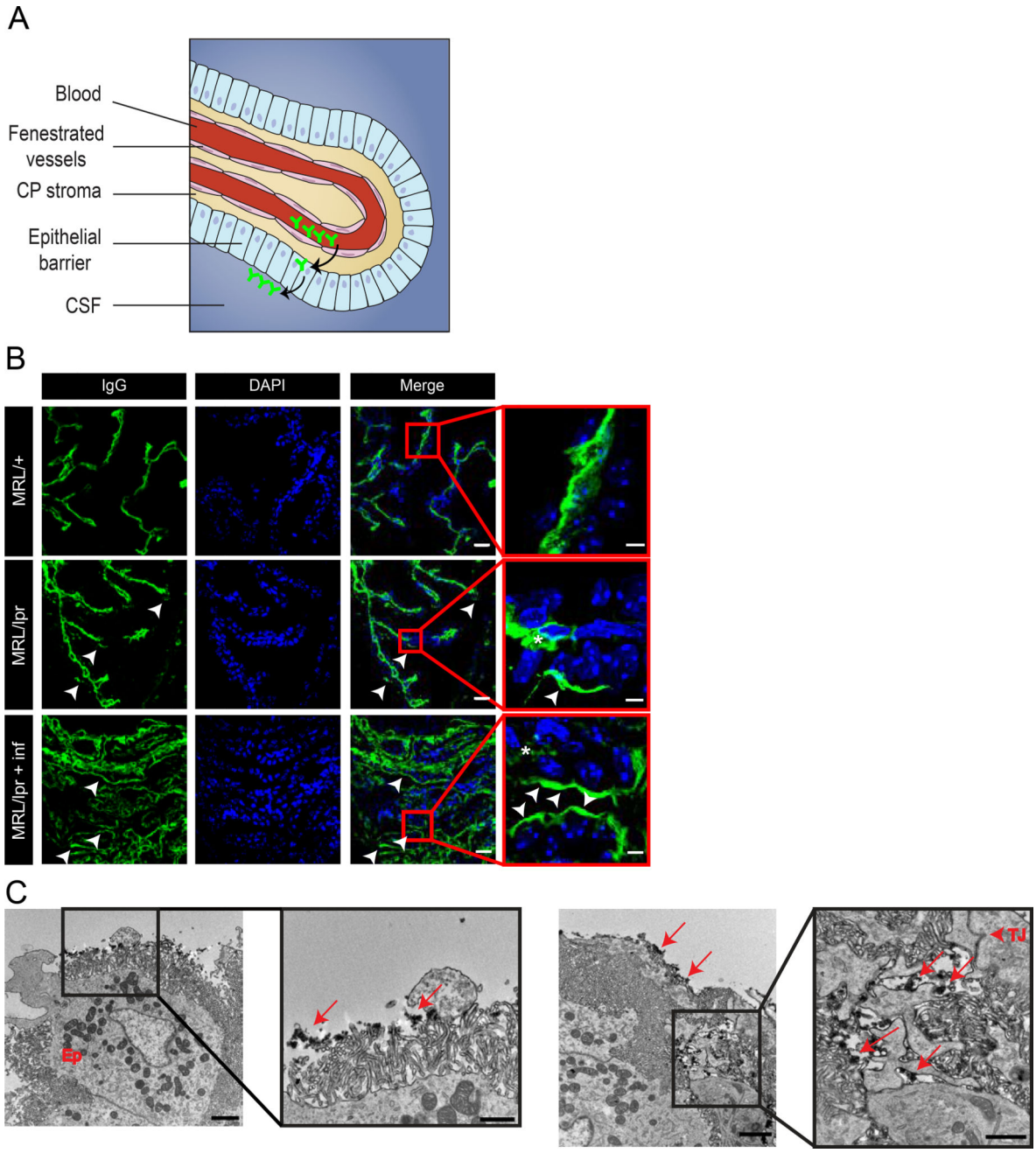

Figure 3. BCSFB dysfunction in NPSLE mice points to an alternative route of antibody entry into the CNS

Examination of endogenous IgG with confocal and TEM imaging indicates abnormal localization of antibodies at the ventricular side of the BCSFB. A. Illustration of the choroid plexus (CP), located in brain ventricles. Tissue structure consists of permeable vessels in the middle and an epithelial barrier at the perimeter of the CP. Antibodies (depicted in green) demarcating the possible route from the blood through fenestrated vessels into the CP stroma and eventually to the apical side of the barrier (modified from[9]). B. Confocal images of 10 μm sagittal brain sections of 16 week old MRL/lpr mice stained for endogenous IgG (green) and nuclei (DAPI, blue). As expected, IgG is found in CP vessels (asterisks). IgG is

also found at the apical side of the epithelial barrier only in 16 week old MRL/lpr mice (lower panels, arrow heads) but not in control MRL/+ mice (upper panel). Ventricular BCSFB IgG staining is more abundant in CP regions where immune cells infiltrated the stroma (highly infiltrated regions, lower panel. less infiltrated regions, middle panel). Scale bars 20 μm and 5 μm in insets. C. TEM imaging of 16 week old MRL/lpr CP stained with IgG-HRP. IgG is localized at the ventricular surface of the BCSFB, covering epithelial cells microvilli (left panel, arrows in inset). Abundant IgG deposits are also found in the basolateral space between epithelial cells (right panel, arrows), reaching the epithelial tight junction (right panel, arrow head in inset). Scale bars 2 μm, and 1 μm in insets.

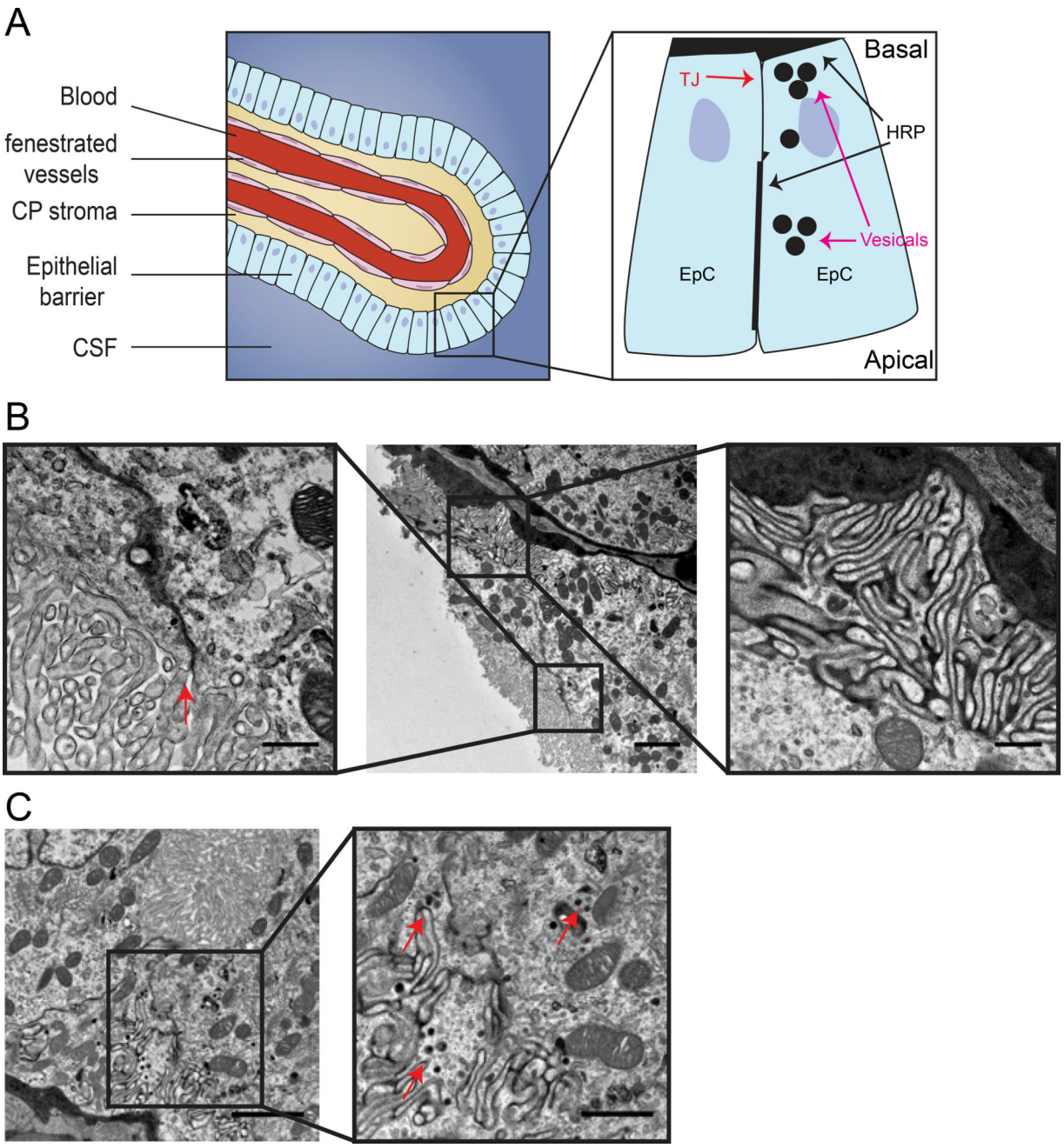

Figure 4. BCSFB dysfunction involves normal function of tight junctions but possible elevation of vesicular activity

Transmission electron microscopy imaging of exogenous tracer challenges in 16 week old MRL/lpr mice. A. Illustration of the BCSFB, inset showing sites of HRP accumulation in the basal side, close to tight junctions and in epithelial vesicles (modified from[9]). B. Large blood vessels surrounded by epithelial cells with HRP at the basement membrane (middle image), HRP in intracellular spaces between epithelial cells (lateral labyrinth, right inset) reaching the level of tight junctions (left inset, arrow). C. Epithelial cell cytoplasm with HRP filed vesicles (right inset, arrows). Scale bars 2 μm and 0.5 μm in inset (B), 1 μm in inset (C).

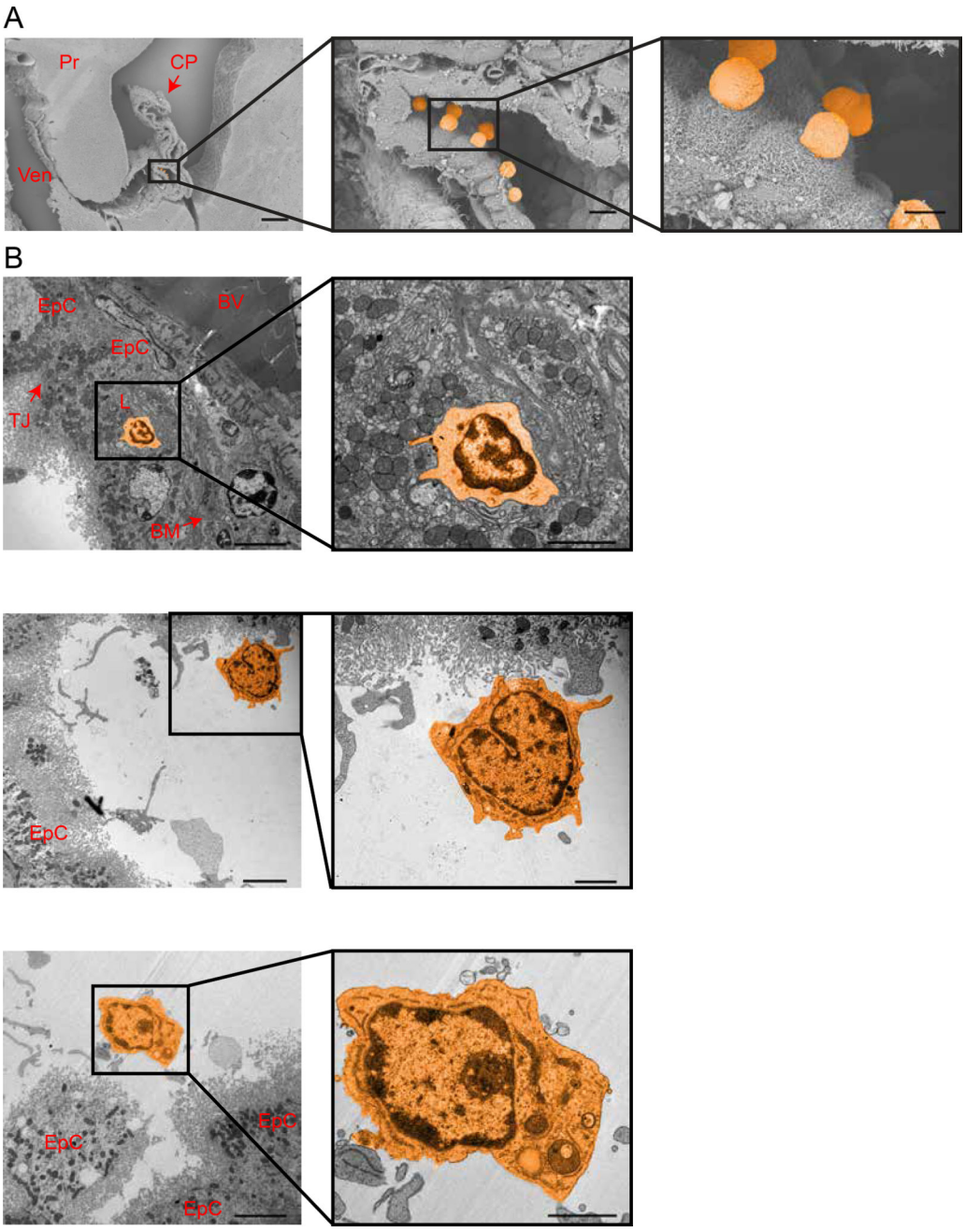

Figure 5. Trans-epithelial passage of immune cells across the BCSFB

NPSLE CP epithelial barrier allows abundant trans-epithelial passage of immune cells. A. Representative scanning electron microscopy images of the CP in 16 week old MRL/lpr mice demonstrating lymphocytes on the ventricular side of the BSCFB (lymphocytes pseudo-labeled in orange). CP=Choroid Plexus, Ven=Ventricle and Pr=parenchyma (Scale bars 280 μm in image and middle inset, and 420 μm in right inset). B. TEM images of the CP in 16 week old MRL/lpr mice demonstrating a lymphocyte (pseudo-labeled in orange) engulfed by an epithelial cell (upper panel) and lymphocytes on the apical side of the

BCSFB. EpC = Epithelial cell, BV = Blood Vessel, TJ = Tight junction, BM = Basement Membrane. Scale bar 5 μm and 2 μm in insets.